Annals of Biomedical Engineering (2024) 52:1009–1020
https://doi.org/10.1007/s10439-023-03437-1

BMES BIOMEDICAL ENGINEERING SOCIETY

ORIGINAL ARTICLE

Functional Assessment of Human Articular Cartilage Using Second Harmonic Generation (SHG) Imaging: A Feasibility Study

Ziad Abusara[1,2] · Eng Kuan Moo[1,4] · Ifaz Haider[1,2] · Claire Timmermann[1] · Sue Miller[2,3,5] · Scott Timmermann[2,3] · Walter Herzog[1,2]

Received: 13 August 2023 / Accepted: 26 December 2023 / Published online: 19 January 2024

Abstract

Many arthroscopic tools developed for knee joint assessment are contact-based, which is challenging for *in vivo* application in narrow joint spaces. Second harmonic generation (SHG) laser imaging is a non-invasive and non-contact method, thus presenting an attractive alternative. However, the association between SHG-based measures and cartilage quality has not been established systematically. Here, we investigated the feasibility of using image-based measures derived from SHG microscopy for objective evaluation of cartilage quality as assessed by mechanical testing. Human tibial plateaus harvested from nine patients were used. Cartilage mechanical properties were determined using indentation stiffness (E_{inst}) and streaming potential-based quantitative parameters (QP). The correspondence of the cartilage electromechanical properties (E_{inst} and QP) and the image-based measures derived from SHG imaging, tissue thickness and cell viability were evaluated using correlation and logistic regression analyses. The SHG-related parameters included the newly developed volumetric fraction of organised collagenous network (Φ_{col}) and the coefficient of variation of the SHG intensity (CV_{SHG}). We found that Φ_{col} correlated strongly with E_{inst} and QP ($\rho = 0.97$ and -0.89, respectively). CV_{SHG} also correlated, albeit weakly, with QP and E_{inst}, ($|\rho| = 0.52$–0.58). E_{inst} and Φ_{col} were the most sensitive predictors of cartilage quality whereas CV_{SHG} only showed moderate sensitivity. Cell viability and tissue thickness, often used as measures of cartilage health, predicted the cartilage quality poorly. We present a simple, objective, yet effective image-based approach for assessment of cartilage quality. Φ_{col} correlated strongly with electromechanical properties of cartilage and could fuel the continuous development of SHG-based arthroscopy.

Keywords Multiphoton laser microscopy · Collagen network · Indentation stiffness · Streaming potential · Osteoarthritis · Knee joint · Bone-cartilage allografts

Associate Editor Michael S. Detamore oversaw the review of this article.

✉ Ziad Abusara
zabusara@ucalgary.ca

Eng Kuan Moo
engkuanmoo@cunet.carleton.ca

Ifaz Haider
ifaz.haider@ucalgary.ca

Sue Miller
shmiller@ucalgary.ca

Scott Timmermann
scotttimmermann@shaw.ca

Walter Herzog
wherzog@ucalgary.ca

[1] Human Performance Laboratory, Faculty of Kinesiology, University of Calgary, Calgary, Canada

[2] McCaig Institute for Bone and Joint Health, Cumming School of Medicine, University of Calgary, Calgary, Canada

[3] Section of Orthopaedic Surgery, Department of Surgery, University of Calgary, Calgary, Canada

[4] Department of Mechanical and Aerospace Engineering, Faculty of Engineering and Design, Carleton University, Ottawa, Canada

[5] Taylor Institute for Teaching and Learning, University of Calgary, Calgary, Canada

Introduction

Osteoarthritis (OA) affects approximately 33% of the population in the United States over the age of 60, with the prevalence increasing with every decade of life thereafter [3, 60]. There is currently no cure for OA once it becomes fully developed. Therefore, research has focused on developing techniques for early detection of OA to allow for early intervention. Some of the hallmarks of early OA are softening and thickening of articular cartilage, surface fibrillation, loss of matrix proteins, and structural changes in matrix proteins [14, 33, 50]. Despite the development of advanced medical imaging systems, arthroscopy remains a standard procedure for joint health assessment [58]. Various techniques that are compatible with arthroscopy have been developed for the measurement of tissue thickness [24, 31], mechanical stiffness [4, 16, 32], surface roughness [17, 51], streaming potentials [9], or laser-induced photoacoustic relaxation times [23]. Of these parameters, mechanical stiffness is the most widely accepted parameter for the assessment of the load-bearing capacity of cartilage [16, 29], and stiffness has been frequently used as the benchmark parameter to evaluate the effectiveness of a newly developed measuring approach or intervention technique [51, 57].

In view of the significant role of mechanical stiffness of articular cartilage, commercial hand-held indenters, such as Artscan^{TM} and Actaeon^{TM}, have been developed for stiffness measurements during arthroscopic procedures [32, 44]. However, these devices require manual indentation within a narrow joint space during *in vivo* assessment, thereby limiting the number of possible measuring points and preventing a holistic assessment of the joint [6]. These experimental limitations may be the cause for a lack of acceptance of hand-held indenters among orthopaedic surgeons [56]. The recently developed hand-held device for the measurement of electromechanical streaming potentials of cartilage (i.e. Arthro-BST^{TM} from Biomomentum Inc.) shows a sensitivity that matches that of an experienced surgeon in making a diagnosis of early OA in the knee [9, 18, 56]. However, similar to the hand-held indenters, measurements with the Arthro-BST require manual indentation, and this requirement may have prevented its widespread use in the orthopaedic field.

Morphological changes of the cartilage surface following injury/degeneration can be measured by imaging methods such as ultrasonography [17, 51], reflectance polarized light microscopy [20–22], and second harmonic generation (SHG) laser microscopy [10, 30, 46]. In particular, the laser-based imaging approaches present an attractive alternative for the non-invasive and non-contact assessment of tissue structure and functional properties at high resolution during arthroscopic procedure [45, 53]. A laser imaging probe can be made of fibre optics with a small diameter (<4 mm) for laser delivery and signal acquisition [5], which facilitates access to narrow joint spaces of 6–7 mm in width [12]. Furthermore, arthroscopic assessment through SHG is not restricted by the orientation of the imaging probe as the light path within the fibre optics filament can be controlled. The recent advances in multiphoton nonlinear microscopy have allowed label-free imaging of collagenous structures through SHG microscopy [10]. SHG microscopy is widely used for the detection of disease-related degeneration of connective tissues, such as cartilages [19, 28, 30, 46], muscles [49], and skin [11]. For example, SHG signal intensity has been shown to correlate positively with the metabolic activity of chondrocytes [7]. Our research group has used SHG microscopy to determine the collagenous structure and cell shapes in cartilage of human allografts [2]. In that study, we noticed a 30% reduced SHG signal in cartilages containing cells with abnormal shapes when compared with cartilages containing normal ellipsoidal cell shapes [2]. It was speculated that the reduction in SHG signal intensity was related to a collagenous disorganisation [52] in the tissue, which may cause tissue softening. However, to our knowledge, the association between SHG-based measures and tissue mechanical properties, such as stiffness, has yet to be established.

The purpose of this study was to investigate the feasibility of using image-based measures derived from SHG microscopy for objective evaluation of the functional quality of human cartilage tissue. Tissue quality was evaluated by quantifying mechanical stiffness and the electromechanical score related to streaming potentials [57]. The correspondence of electromechanical properties of cartilage and quantitative measures derived from SHG imaging were systematically tested using correlation and logistic regression analyses. In addition, tissue thickness [15] and cell viability [8] as predictors of mechanical degeneration in cartilage were also investigated. We hypothesised that the image-based measures derived from SHG microscopy are related to the electromechanical properties of cartilage and therefore can be used as an effective alternative for grading tissue quality.

Materials and Methods

Tissue Procurement

This research was approved by the University of Calgary Conjoint Health Research Ethics Board and Alberta Health Services. Fresh tibial plateaus were harvested from patients undergoing surgery for total knee replacement (N = 9; 2

male, 7 female; age: 64.1 ± 7.5 years) at the Peter Lougheed Hospital in Calgary, Canada. Samples were kept in a phosphate-buffered saline (PBS) solution and delivered to the university laboratory within 2–4 h for testing. The workflow of the testing is summarised in Fig. 1.

Identification of Measurement Points

The tibial plateau samples were rigidly embedded in a sample holder filled with PBS. Two reference points were selected from consistent anatomical locations at the edge of the tibial plateau and marked with a 23-gauge needle dipped in methylene blue stain. A position grid of 25 columns by 19 rows with an inter-grid spacing of 3.33 mm was generated. The position grid was aligned with the two marked reference points and overlaid over the top surface of the samples by a camera registration system (Mapping Toolbox, Biomomentum Inc., Canada). The grid points represent the measurement points for the imaging, electromechanical testing, indentation application, and thickness measurements. A total of 394 measurement points were studied (28–69 points per joint). These points were marked using a fine-point permanent marker (Sharpie, GA, United States) to facilitate cross referencing when transitioning from one measurement type to another.

Multi-photon Imaging of Live/Dead Cells and Collagenous Network

Samples were fluorescently stained using 2 µM calcein AM and 4 µM ethidium homodimer-1 (both from Molecular Probes/ Invitrogen, USA) for 30 min for live and dead cells, respectively [2]. Samples were washed using PBS thrice to remove excessive staining before being fixed in a sample holder filled with fresh PBS for multiphoton laser imaging. For imaging, a multiphoton microscope (model FVMPE-RS, Olympus, Japan) coupled with two independent infrared pulsed lasers (InSight DS and Mai Tai DeepSee, Spectra Physics Inc., USA) was used. Specimens were imaged using a 25×, 1.05 NA water-immersion objective. The collagen fibrous network was imaged label-free at 800 nm using second harmonic generation (SHG) imaging. Live/

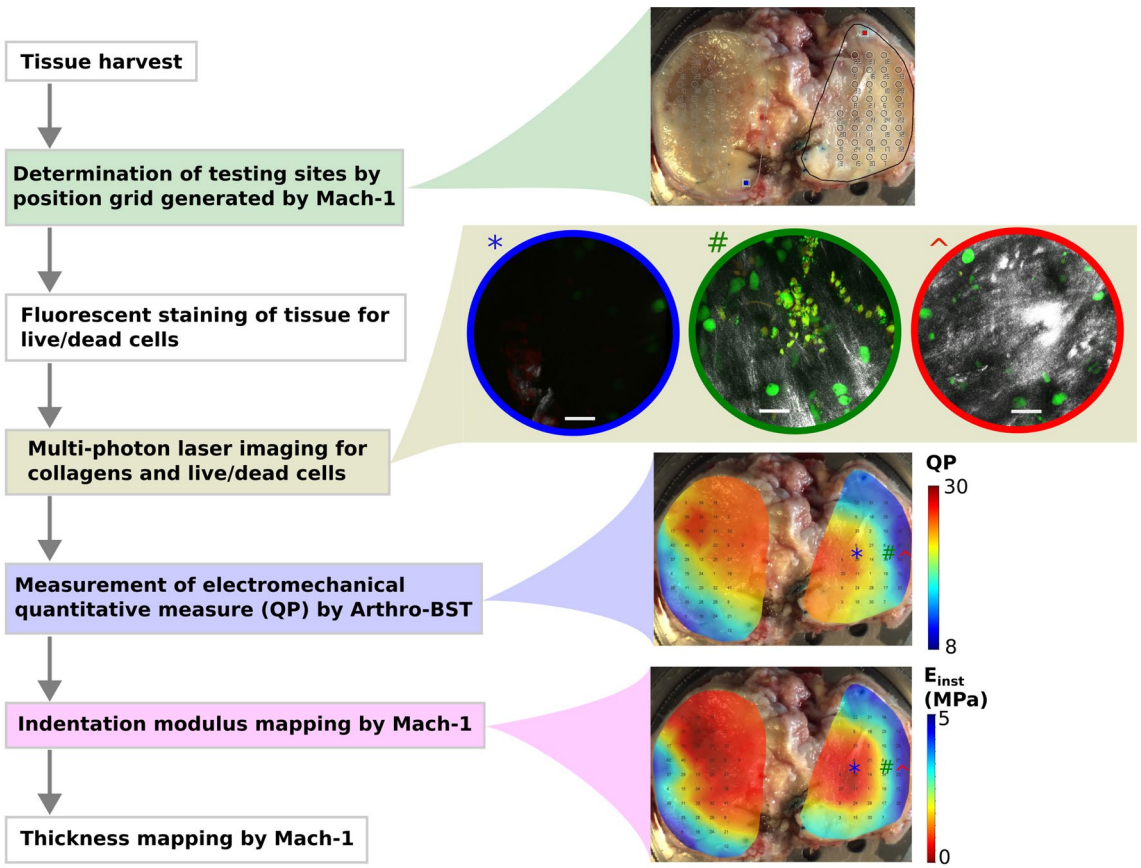

Fig. 1 Workflow of the current study. Representative example of a tested tibial plateau showing the relationship between tissue stiffness (E_{inst}), electromechanical properties (QP), cell shape (green ellipse), and volume fraction of organised collagen network (grey signal) for different tissue groups (0–2) in the order of increasing disease severity, with group 0 being the healthy tissue. Tissue regions that were categorised as tissue group 0, 1 and 2 are marked by ^, # and *, respectively. Scale bar: 40 µm.

dead cell imaging was performed using a two-photon fluorescence (TPF) technique at 940 nm [35, 42]. The emission signals were collected in the epi-direction and were passed through a single-edge dichroic beam splitter (FF458-Di02, Semrock inc., USA) to separate the SHG signals from the TPF signals at a wavelength of 458 nm. The TPF signals were further split into live cell and dead cell signals by a dichroic beam splitter of 570 nm (FF570-Di01, Semrock inc. USA). Finally, the live/dead cell images were collected in two separate channels by two non-descanned detectors using bandpass filters (FF01-520/35 and FF01-612/69, Semrock inc., USA) at 520 nm and 612 nm, respectively. The SHG signal was collected by a GaAsp non-descanned detector after being bandpass filtered at 400 nm (FF01-400/40, Semrock inc., USA) [1, 2].

Stacks of multi-channelled 509×509 μm^2 images (pixel size: 0.994 μm × 0.994 μm; dwell time: 2 μs; scan time/frame: 1.08 s, bit-depth: 12) were acquired at 1 μm z-increment from the articular surface to a depth of 100–120 μm. Image acquisition rate was 0.9 s/frame. Each image stack took approximately 90–100 s to image.

Electromechanical Mapping

A hand-held Arthro-BST^{TM} instrument (Biomomentum Inc., Canada) was used to measure the electromechanical properties of the cartilage covering the tibial plateaus. This device consists of a hemi-spherical indenter (diameter: 6.35 mm) that is covered with an array of 37 microelectrodes (5 electrodes/mm^2) in order to measure the streaming potentials resulting from tissue indentation. The cartilage was manually indented by the Arthro-BST^{TM} instrument for 1 s to measure the so-called 'quantitative parameter' (*QP*), which is defined as the number of microelectrodes that are required to make contact with the articular cartilage in order to attain a total streaming potential of 100 mV. The unique design and outcome measure QP of the Arthro-BST device ensure that the electromechanical measurements are independent of the surface orientation and tare load [56]. The *QP* is inversely proportional to the streaming potential [56]. The *QP* is a validated parameter and is robust against measuring noises when compared to direct measurement of streaming potentials [56]. QP was measured three times at each pre-defined measurement point location (see Section "Identification of Measurement Points").

Automated Indentation Mapping

Articular cartilage indentation was automated by using an indentation device (Mach-1, v500css, Biomomentum Inc., Canada) instrumented with a multi-axial load cell (range: 70N; resolution: 3.5 mN). A spherical indenter with a diameter matching that of the Arthro-BST^{TM} device was used. Surface contact was established by a tare load of 4 mN applied at a loading rate of 0.1 mm/s. The surface normal was calculated automatically by the Mach-1 device from the coordinates of four surrounding points (±0.3 mm in the x- and y-directions) determined by a brief indenter contact. The pre-defined measurement points were then indented to a depth of 400 μm at a rate of 200 μm/s normal to the cartilage surface.

Automated Thickness Mapping

Local tissue thickness was measured using the 'needle probe' technique [25, 39, 43]. Briefly, a bevelled needle (26G 3/8" Precision-Glide, intradermal) was attached to the Mach-1 system and moved perpendicularly to the cartilage surface at a constant speed of 0.1 mm/s piercing the cartilage. The movement of the needle was automatically halted when the reaction force exceeded a set threshold value, reflecting that the needle had encountered the subchondral bone. The cartilage thickness was then calculated from the force-displacement curve accounting for the orientation of the surface normal [55].

Data Analysis

Instantaneous Modulus (E_{inst})

Using the thickness values measured in Section "Automated Thickness Mapping", the curve of indentation stress against percentage of tissue thickness was plotted. The instantaneous modulus, E_{inst}, was determined from the indentation loading curve as the tangent modulus at a strain of 10% of the nominal tissue thickness. The distribution of E_{inst} over the articular surface was interpolated into a coloured heatmap by using the Mapping Toolbox software (MT337 v1.5.0.4, Biomomentum Inc., Canada), with red and blue colours indicating low and high E_{inst}, respectively (Fig. 1).

Quantitative parameters (QP)

The distribution of QP over the articular surface was also interpolated into a coloured heatmap by using the Mapping Toolbox software, with red and blue colours indicating high and low QP, respectively (Fig. 1).

Image Processing for Φ_{col}, CV_{SHG} and *Cell Viability*

The multi-channelled images acquired in Section "Multi-photon Imaging of Live/Dead Cells and Collagenous Network" were split into their respective channels as image stacks of SHG collagens, live cells and dead cells for further processing by a custom Matlab code [2]. The SHG images were first de-noised using a Gaussian filter with the standard

deviation of the Gaussian distribution set at 7 pixels. Due to the specificity of SHG imaging to highly ordered crystalline structures that lack inversion symmetry [34, 53, 59], the collected SHG signals were attributed to the organised collagen fibrous network. The tissue volume containing organised collagen networks, V_{col}, was determined by a threshold segmentation procedure with the cut-off threshold set at 30% of the maximum intensity [2, 35] (see Supplementary Materials, S1 for details). The total tissue volume, V_{tissue}, was calculated from the thresholded region after filling all empty discontinuities within the region by using the Matlab 'imfill' function. A new objective measure known as the volumetric fraction of the organised collagenous network, Φ_{col}, was defined as the ratio of V_{col} to V_{tissue}. In addition, the dispersion of the SHG intensity within the V_{tissue} was calculated in terms of a coefficient of variation (CV_{SHG} = standard deviation/mean).

The volumes of live and dead cell nuclei were determined from the respective image stacks by using a cut-off threshold of 30% maximum intensity that was specific to each image stack [35] (see Supplementary Materials, S1 for details). As the cartilage specimens were affected by different degrees of osteoarthritis progression, the morphology of many cells was abnormal (see Fig. 5 of Abusara et al. [2] for examples), making it challenging to perform cell counting. Therefore, cell viability was defined as the volume percentage of live cells relative to all cells (i.e. live and dead cells).

Statistical Analysis

The commercial statistical package SPSS (version 27, SPSS Inc. IL, USA) was used for statistical analysis. Previous studies found high correlations between the electromechanical QP and the International Cartilage Repair Society (ICRS) grade, which is regarded the gold standard evaluation system for arthroscopic assessment [18, 56, 57]. Therefore, the current data were divided into three groups based on the QP values (group 0: $QP \leq 13$, group 1: $13 < QP \leq 21$, and group 2: $QP > 21$), which is equivalent to the ICRS grades of 0, 1 and 2, respectively [18, 56, 57]. The objective measures of E_{inst}, Φ_{col}, CV_{SHG}, cell viability and local tissue thickness were compared for between-group effects using a generalised estimating equation (GEE, under the Genlin procedure in SPSS) to take into account the unbalanced design (i.e. unequal number of measurement points between specimens) of the study. As the Shapiro–Wilk test of normality indicated that the data of all outcome measures were not normally distributed, the correlation between the objective measures (i.e. E_{inst}, Φ_{col}, CV_{SHG}, QP, cell viability and local tissue thickness) was assessed using the non-parametric Spearman's rank-order test. The coefficient of determination and the associated 95% two-sided confidence intervals and prediction limits were calculated for reference.

Logistic regression analysis was also conducted to evaluate the potential of using the tested objective measures for classification of tissue regions into the corresponding disease state. Briefly, 70% data of each objective measure were randomly selected and used to train the logistic regression model available in the *Scikit-learn* python module [48], with the remaining 30% of the data used to evaluate the classification efficiency. The receiver-operating characteristic (ROC) curves of the 0-1, 1-2 and 0-2 group classification, and the corresponding area under the curve (AUC), were determined [47]. The AUC reflects the performance of an objective measure, with a value of 1.0 indicating a 100% prediction accuracy, and a value ≤ 0.5 indicating random guessing. The procedure was repeated ten times with different data randomisation and the average value of the AUC was reported. The significance level of all statistical tests was set a priori at $\alpha = 0.05$. Results are presented as estimated marginal means $\pm$ 1 standard error (SE).

Results

The relationship between tissue stiffness (E_{inst}), electromechanical properties (QP), cell shape (green ellipse), and volume fraction of organised collagen network (grey signal) is illustrated graphically in Fig. 1. The joint surface with low E_{inst} and high QP (marked by the blue circle, Fig. 1) had few live cells and low Φ_{col}, whereas the joint surface with high E_{inst} and low QP (marked by the red circle, Fig. 1) had chondrocytes with normal ellipse shape, and high Φ_{col}.

Correlation

The results of all correlation tests are summarised in Table 1. Graphs of selected objective parameters showing strong correlations are included in Fig. 2 and 3. E_{inst} correlated strongly with Φ_{col} ($\rho = 0.97$), and QP correlated strongly with E_{inst} and Φ_{col} (each with $\rho = -0.89$). Although CV_{SHG} showed significant correlation with QP, E_{inst}, and Φ_{col}, the correlations were moderately strong with $|\rho|$ ranging from 0.52 to 0.58. Tissue thickness and viability showed little or no correlation with E_{inst} and QP, respectively (Table 1).

Logistic Regression

The performance of every objective measure in classifying the tissue region in terms of tissue quality is summarised in Table 2, with the results of the full analysis provided in the Supplementary Materials, S2. The ROC curve and the corresponding AUC values are presented in Figure 4. E_{inst} and Φ_{col} are found to be strong predictors of tissue quality and could be used to distinguish healthy tissue (group 0) from tissues of varying degree of degeneration (group 1 and

Table 1 Spearman rank-order correlations and the fitted equations of the correlation analyses between all objective measures

X-variable \ Y-variable	E_{inst}	Φ_{col}	CV_{SHG}	Thickness, h	Viability, α
E_{inst}		0.97* $\Phi_{col}=0.081E_{inst}+0.007$	-0.58* $CV_{SHG}=e^{-0.158}E_{inst}^{-0.101}$	0.12* $h=0.017E_{inst}+1.81$	0.03 –
QP	-0.89* $E_{inst}=e^{-0.197QP+3.14}$	-0.89* $\Phi_{col}=e^{-0.323QP+2.37}$	0.52* $CV_{SHG}=e^{0.021QP-0.495}$	-0.08 –	0.04 –
Φ_{col}			-0.58* $CV_{SHG}=e^{-0.067}\Phi_{col}^{-0.342}$	0.09 –	0.00 –
CV_{SHG}				-0.08 –	-0.14* $\alpha=-21.8CV_{SHG}+100$
Thickness, h					0.01 –

*indicates significant correlation. The E_{inst}-Φ_{col} pair showed the strongest correlation ($\rho=0.97$), followed by the pairs of QP-E_{inst} and QP-Φ_{col} (both showing $\rho=-0.89$).

group 2) with AUC > 0.90. CV_{SHG} predicted tissue quality moderately well, with average AUC between 0.70 and 0.87 (Table 2). However, tissue thickness and cell viability were poor predictors of tissue quality, with AUC around 0.50 (i.e. random guessing).

Comparison of Tissue Groups with Varying Severity of OA

Cartilage region belonging to tissue groups 1–2 showed surface fibrillation and erosion (Fig. 1). Of the 394 measurement points, 153 were determined to be in tissue group 0, while 177 and 64 of them fell into tissue groups 1 and 2, respectively. E_{inst}, Φ_{col}, and CV_{SHG} changed significantly with cartilage degeneration, whereas cell viability and tissue thickness were relatively constant across all tissue groups (Fig. 5).

Discussion

The primary goal of this study was to investigate the potential use of SHG imaging for objective assessment of the functional quality of human articular cartilage. From our data, we confirm the inverse relationship between the instantaneous stiffness E_{inst} and the electromechanical QP (Fig. 2, Table 1) that was established in previous studies [56]. Both E_{inst} and QP reflect the functional properties of cartilage, and they require tissue indentation for assessment. In contrast, the SHG imaging offers a non-contact measuring technique that may prove powerful for functional assessment of allografts and future clinical applications in the form of an arthroscope [5, 27]. While multiphoton SHG imaging is known to provide structural information of the tissue [11, 19, 28, 30, 34, 49, 53, 54], its relevance in characterising accurate cartilage mechanical function had not been tested systematically. We attempted to fill this knowledge gap by measuring the correlation between the SHG-derived measures (CV_{SHG} and Φ_{col}) with the electromechanical properties of human cartilages. Our results show that (i) the Φ_{col} correlated strongly with E_{inst} ($\rho=0.97$, $p<0.01$), and QP ($\rho=-0.89$, $p<0.01$), (ii) the CV_{SHG} also correlated with QP, E_{inst}, but to a lesser degree ($|\rho| = 0.52 - 0.58$), (iii) by using QP scores to group the tissues into regions of degrees of degeneration, E_{inst} and Φ_{col} were found to be the most sensitive predictors of cartilage health quality with AUC > 0.90 (Fig 4, Table 2), whereas CV_{SHG} only showed moderate sensitivity (AUC = 0.7), and (iv) cell viability and tissue thickness, often used in the past [8, 15], were poor predictors of cartilage quality (Fig. 4, Table 2).

E_{inst}, QP, and Φ_{col} quantify different aspects of cartilage properties. E_{inst} measures the mechanical stiffness of the fibre-reinforced, proteoglycan-filled cartilage matrix [36, 38, 43]. QP is related to the compression-induced streaming potentials [56, 57]. In contrast, Φ_{col} is a newly developed parameter providing insights into the volume of tissue containing organised collagenous networks (see Methods for more details). Interestingly, despite measuring these seemingly different properties and quantities of the articular cartilage samples, these parameters showed strong negative ($\rho=-0.89$) and positive ($\rho=0.97$) correlations with each other. The lower correlation strength with QP ($\rho=-0.89$, Fig. 2A, 2C) was likely caused by the increasing difficulty of harnessing enough streaming potential (> 100 mV) for degenerated tissues with QP scores > 22 (Fig. 2A and 2C). Nevertheless, our results suggest that an image-based parameter (Φ_{col}) is robust and reliable in providing accurate information on the functional capacity of articular cartilage.

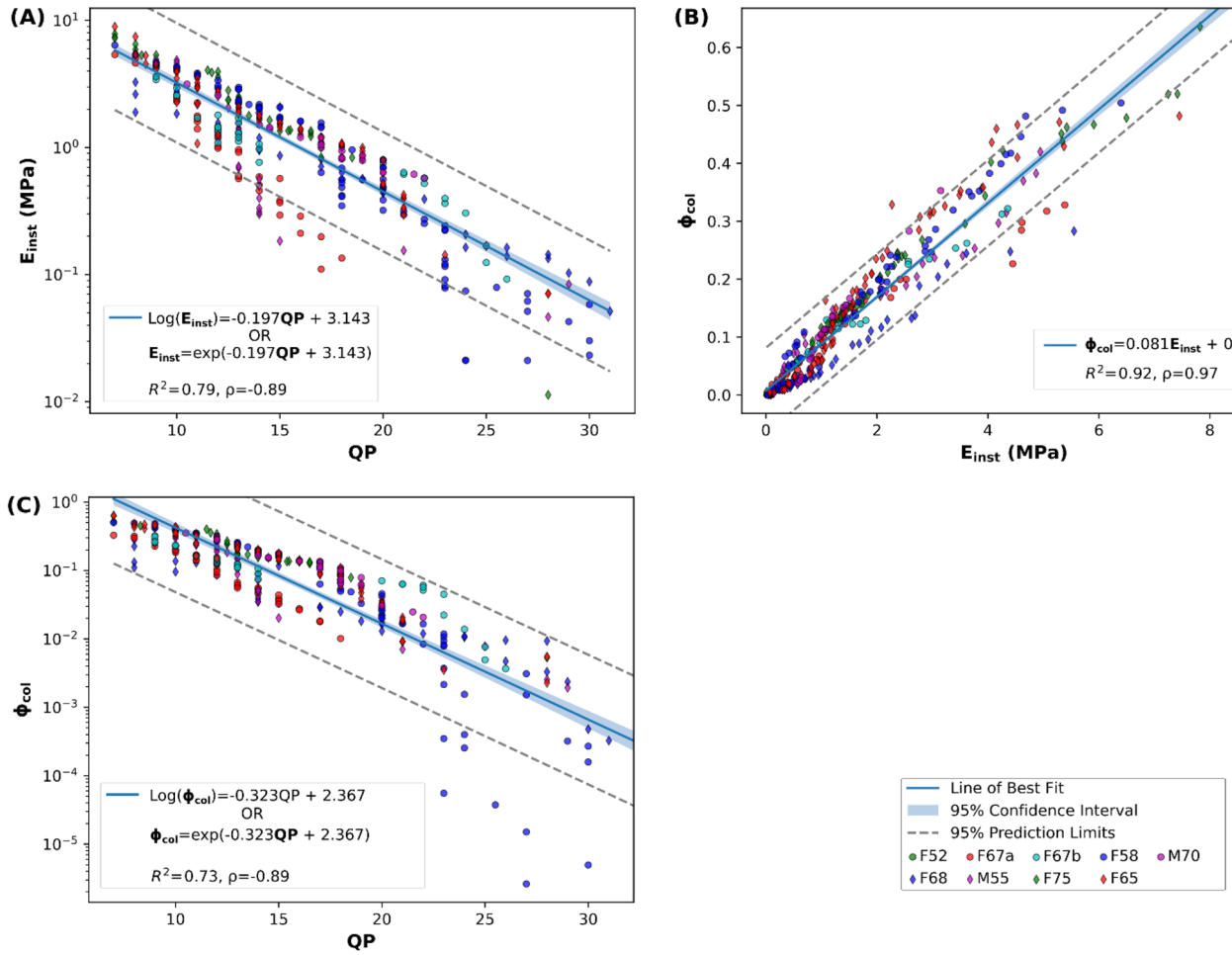

Fig. 2 Correlations between **A** instantaneous modulus E_{inst} vs. electromechanical quantitative parameter QP, **B** volumetric fraction of the organised collagenous network Φ_{col} vs. E_{inst}, and **C** Φ_{col} vs. QP. A total of 394 data points were collected, with data from each patient labelled with different colours. Sex (M: male, F: female) and age are provided in the figure legend. The best-fit lines are shown in blue, the 95% confidence intervals are indicated with the light blue shaded area around the blue line, and the 95% prediction limits are designated with the dashed lines. The Spearman's coefficient, ρ, the coefficient of determination, r^2, and the fitted equations are also presented. Note that the y-axes in (**A**) and (**C**) are of logarithmic scale. All correlations were statistically significant ($p < 0.05$).

In the past, various attempts have been made to apply image-based approaches, such as laser imaging and ultrasonography, for the assessment of cartilage quality and functional capacity at different stages of OA [2, 17, 19, 23, 28, 30, 51]. While promising at the time, few of them provided a direct relationship with the mechanical function of cartilage. For example, SHG signal intensity has been shown to correlate with cell metabolic activity [7]. Increased dispersion of SHG signals was shown to be related to abnormal cell shape [2] and tissues with OA-like features [28]. Ishihara et al. [23] found positive correlations between the photoacoustic viscoelastic relaxation time of cartilage and the duration of trypsin treatment, but fell short at providing direct comparison with the mechanical properties of the cartilage. In studies in which functional capacity of cartilage was compared to image-based parameters, the corresponding correlations were moderate at best. For example, Saarakala et al. [51] and Gelse et al. [17] discovered moderate correlations (ρ of 0.47–0.65) between ultrasonography-derived measures and dynamic stiffness of articular cartilage.

SHG imaging is a versatile tool to study the structural properties of tissue matrix and its interaction with the cells [30, 34, 41, 42]. The SHG signals arise from the non-centrosymmetric collagen fibres and the dipoles associated with the peptide bond structure of the collagen [34, 53, 59]. The emitted SHG signals depend on the orientation of the collagen fibres and are strongest when the collagen fibres lie in the imaging plane and align with the polarisation of the exciting laser beam. Therefore, SHG signals become weaker when the orientation of the collagen fibre network does not satisfy these two conditions. By taking advantage of the fact that the collagen network undergoes substantial

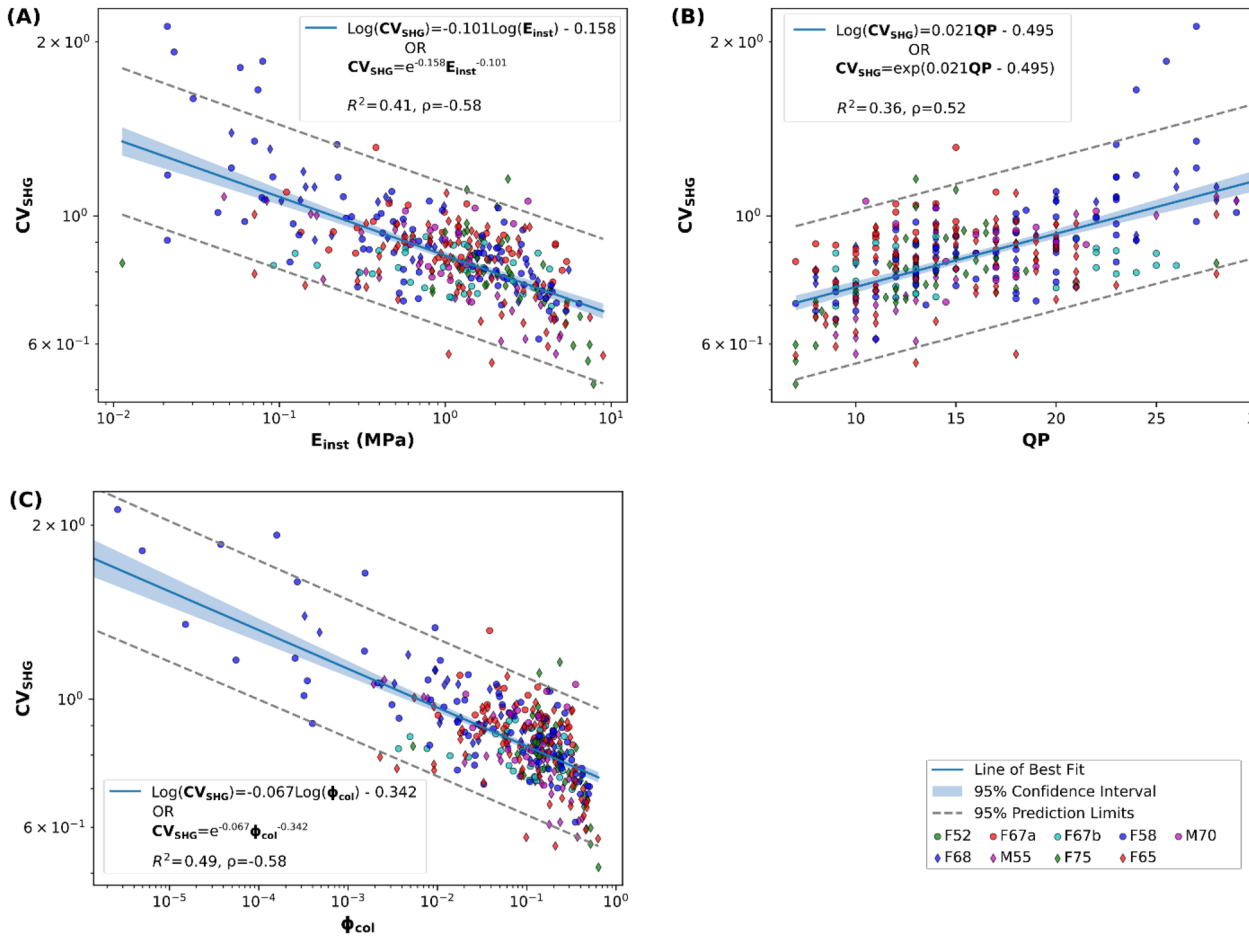

Fig. 3 Correlation between the CV of the SHG intensity, CV_{SHG}, with **A** E_{inst}, **B** QP, and **C** Φ_{col}. The graph layout is the same as in Fig. 2. Note that the x - and y axes of all graphs, but the x axis of (**B**), are of logarithmic scale. All correlations were statistically significant ($p < 0.05$).

Table 2 Mean (± 1 standard deviation) values of the area under the curve (AUC) obtained from ten simulated runs of the logistic regression for every objective measure (see Methods for more details).

Group comparison	E_{inst}	ϕ_{col}	CV_{SHG}	Viability	Thickness
0 vs. 1	0.91 ± 0.03	0.90 ± 0.03	0.70 ± 0.05	0.48 ± 0.04	0.49 ± 0.06
1 vs. 2	0.93 ± 0.02	0.96v0.02	0.76 ± 0.04	0.48 ± 0.06	0.64 ± 0.07
0 vs. 2	1.00 ± 0.00	1.00 ± 0.00	0.87 ± 0.04	0.55 ± 0.08	0.58 ± 0.04

disorganisation during early OA [14, 33, 38], with the superficial collagen fibrous orientation changing from mainly parallel (0-5°) to mainly oblique (20–35°) relative to the articular surface [13, 14], thereby affecting the strength of the SHG signals, we applied a thresholding method to obtain the volumetric fraction of the organised collagenous network, Φ_{col}. It was exciting to discover the incredibly strong correlation of Φ_{col} with E_{inst} and QP. Our interpretation of the physiological meaning of Φ_{col} is also consistent with previous studies, which showed that collagen fibrous network disorganisation is associated with a concomitant decrease in cartilage stiffness [14, 38] and an increase in QP [18] with the progression of OA.

We further assessed the sensitivity of Φ_{col} in distinguishing healthy and diseased tissue quality. As our study design required the testing of fresh specimens harvested from orthopaedic surgeries, we were unable to arrange for ICRS grading of our samples. Since QP has been shown to be a potent surrogate measure of the ICRS grades ($\rho = 0.86$ as in Hadjab et al. [18]), we divided our data into three groups based on the measured QP, which corresponded to ICRS grades 0–2 [18, 57]. Our results suggest that Φ_{col} was as sensitive as E_{inst}

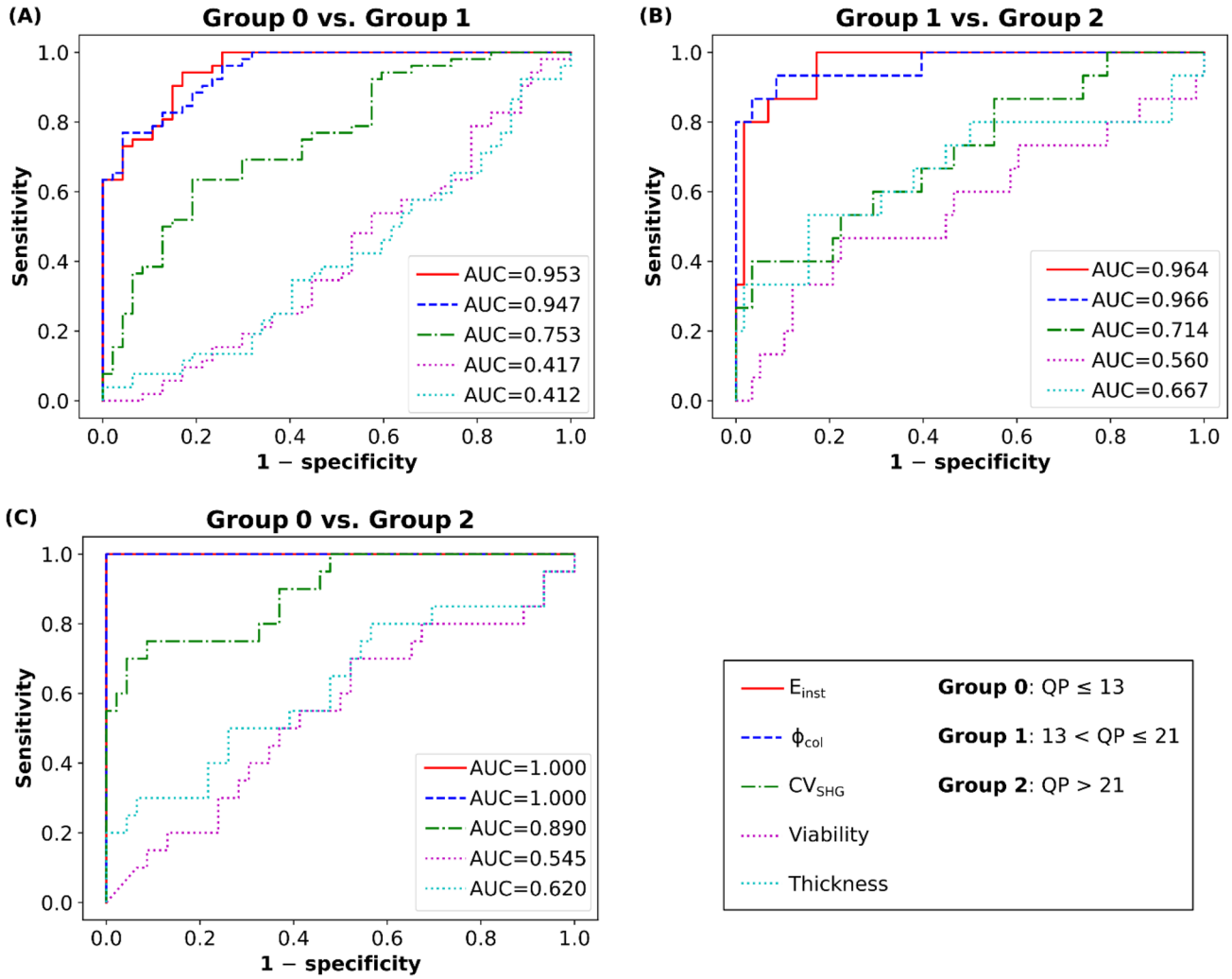

Fig. 4 Receiver operating characteristic (ROC) curves and the corresponding area under the curve (AUC) showing the performance of each of the five objective measures (E_{inst}, Φ_{col}, CV_{SHG}, QP, cell viability and local tissue thickness) in the binary classification of the tissue region into healthy region (group 0) and degenerated regions of increasing severity (group 1 & 2, see Methods for more details). Note that an AUC value of 1.0 indicates a 100% prediction accuracy whereas an AUC value of ≤ 0.5 denotes random guessing.

in classifying the tissue into different quality grades with prediction accuracy of > 90% (AUC > 0.90, see Methods for definition). We note that not every quantitative measure derived from SHG imaging was as good as Φ_{col}. The CV_{SHG}, which was found to be related to OA development in small animal models [28], only showed moderate prediction accuracy of 70–87% in our human tissues. The predictive performance of other variables, such as cell viability and tissue thickness [8, 15], was equivalent to random guessing (Table 2, Fig. 4).

There are limitations to this study that should be considered when interpreting the results and drawing conclusions. Firstly, the cell viability reported here represents the volume percentage of live cells relative to all (live and dead) cells, rather than the conventional method that counts the number of live/dead cells. Also, only the volume of the dead cell nuclei was accounted for. The current quantification method was used as it was hard to perform cell counting since the boundary of the abnormal cells with multiple cytoplasmic projections was hard to define [2]. This may cause overestimation of the cell viability compared to conventional methods based on cell counting. Since it was applied systematically to all data, it should still correlate with electromechanical variables, if such a relationship indeed exists. Secondly, only human tibial plateaus were investigated here. Since it is known that cartilage material properties and cartilage degradation depend on the location within the joint [57], future studies should focus on determining whether the current findings can be extrapolated to other regions of the knee, such as the femoral condyles, the femoral groove, and the retro patellar surface. Thirdly, the tissue regions were graded based on the measured QP rather than based

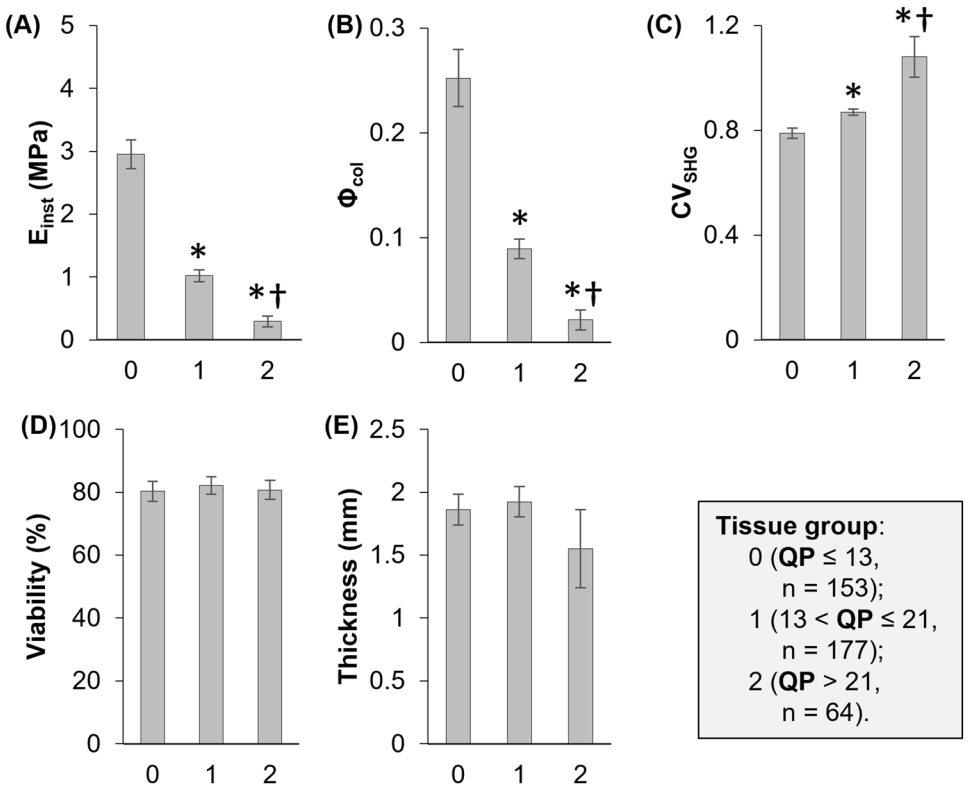

Fig. 5 Estimated marginal mean (± 1 SE) values of **A** E_{inst}, **B** Φ_{col}, **C** CV_{SHG}, **D** cell viability, and **E** local tissue thickness, as a function of tissue group, which corresponds to the ICRS grade [57] (0–2 in the order of increasing disease severity, with group 0 considered a healthy tissue region). The values E_{inst}, Φ_{col} and CV_{SHG} changed significantly with cartilage degeneration, whereas cell viability and tissue thickness remained unchanged with tissue groups. * and † indicate the statistical difference when compared with tissue group 0 and group 1, respectively.

on evaluation by experienced orthopaedic surgeons. We believe that the tissue grading used here (i.e. groups 0–2) is acceptable due to the excellent agreement between *QP* scores and the standard ICRS grading [18, 57]. Fourthly, the Φ_{col} was only measured using a single excitation wavelength of 800 nm. The dependence of Φ_{col} on other SHG excitation wavelengths was not studied. Finally, we only assessed the Φ_{col} for conditions where the direction of the laser beam was perpendicular to the articular surface. Considering the narrow joint space available for *in vivo* arthroscopic assessment, it may be challenging to always perform perpendicular beam-surface alignment and for all locations in an intact human knee. Therefore, the sensitivity of Φ_{col} to beam-surface alignment should be investigated further. In addition, future studies should investigate the relationship between the Φ_{col} and the cellular properties, such as the shape [2], population density [26], metabolic activities [7], and membrane morphology [37, 40]. Such studies may improve our understanding of *in situ* cell mechanobiology.

Conclusion

In summary, we present a simple, objective, yet effective image-based approach for the assessment of cartilage functional properties, cartilage health and quality. The imaging derived parameter Φ_{col} provides an additional structural index for cartilage and is shown to correlate strongly with tissue stiffness and streaming potential-based measures, thereby showing great promise for translation into clinical settings for human joint health assessment in the near future. Nevertheless, additional investigations are warranted to evaluate the efficiency of Φ_{col} under different and clinically relevant testing conditions. We hope that the current findings can stimulate the orthopaedic field to further explore the potential of using multiphoton laser imaging for early OA detection in the human knee.

Acknowledgements We would like to express our gratitude to Ms. Christiana Choi who helped in tissue procurement from arthroplasty procedure, the PLC, Surgical Suite, and Mr. Azim Jinha who provided technical support during data analysis.

Author Contributions (1) The conception and design of the study, or acquisition of data, or analysis and interpretation of the data: ZA, EKM, IH, CT, SM, ST and WH. (2) Drafting the article or revising it critically for important intellectual content: ZA, EKM, IH, CT, SM, ST and WH. (3) Final approval of the version to be submitted: ZA, EKM, IH, CT, SM, ST and WH.

Funding This study was supported by the Joint Transplantation Program at the McCaig Institute for Bone and Joint Heath, University of Calgary, the Calgary Health Trust, the Carleton University internal start-up research fund (186725), the Natural Sciences and Engineering Research Council of Canada (NSERC) Discovery grant (funding reference no: DGECR-2023-00346), The Killam Foundation, The Canadian Institutes of Health Research, and the Nigg Chair for Mobility and Longevity.

Declarations

Conflict of interest The authors declare that there is no conflict of interest.

References

1. Abusara, Z., S. H. J. Andrews, M. V. Kossel, and W. Herzog. Menisci protect chondrocytes from load-induced injury. *Sci. Rep.* 8:14150, 2018.
2. Abusara, Z., I. Haider, E. K. Moo, S. Miller, S. Timmermann, and W. Herzog. Chondrocyte morphology as an indicator of collagen network integrity. *Connect Tissue Res.* 63:319–328, 2022.
3. Anderson, A. S., and R. F. Loeser. Why is osteoarthritis an age-related disease? *Best Pract. Res. Clin. Rheumatol.* 24:15, 2010.
4. Bae, W. C., M. M. Temple, D. Amiel, R. D. Coutts, G. G. Niederauer, and R. L. Sah. Indentation testing of human cartilage: sensitivity to articular surface degeneration. *Arthritis Rheumatism*. 48:3382–3394, 2003.
5. Baskey, S. J., M. Andreana, E. Lanteigne, A. Ridsdale, A. Stolow, and M. E. Schweitzer. Pre-clinical translation of second harmonic microscopy of meniscal and articular cartilage using a prototype nonlinear microendoscope. *IEEE J. Transl. Eng. Health Med.* 7:1–11, 2019.
6. Brama, P. A., A. Barneveld, D. Karssenberg, G. P. Van Kampen, and P. R. Van Weeren. The application of an indenter system to measure structural properties of articular cartilage in the horse. Suitability of the instrument and correlation with biochemical data. *J. Vet. Med. Ser. A*. 48(4):213–21, 2001.
7. Brockbank, K. G. M., W. R. MacLellan, J. Xie, S. F. Hamm-Alvarez, Z. Z. Chen, and K. Schenke-Layland. Quantitative second harmonic generation imaging of cartilage damage. *Cell Tissue Bank*. 9:299–307, 2008.
8. Bugbee, W. D., A. L. Pallante-Kichura, S. Görtz, D. Amiel, and R. Sah. Osteochondral allograft transplantation in cartilage repair: graft storage paradigm, translational models, and clinical applications. *J. Orthop. Res.* 34:31–38, 2016.
9. Changoor, A., J. P. Coutu, M. Garon, E. Quenneville, M. B. Hurtig, and M. D. Buschmann. Streaming potential-based arthroscopic device is sensitive to cartilage changes immediately post-impact in an equine cartilage injury model. *J. Biomech. Eng.* 133(6):061005, 2011.
10. Chen, X., O. Nadiarynkh, S. Plotnikov, and P. J. Campagnola. Second harmonic generation microscopy for quantitative analysis of collagen fibrillar structure. *Nat. Protocols*. 7:654–669, 2012.
11. Cicchi, R., D. Kapsokalyvas, V. De Giorgi, V. Maio, A. Van Wiechen, D. Massi, T. Lotti, and F. S. Pavone. Scoring of collagen organization in healthy and diseased human dermis by multiphoton microscopy. *J. Biophoton.* 3:34–43, 2010.
12. Dacre, J. E., D. L. Scott, J. A. Da Silva, G. Welsh, and E. C. Huskisson. Joint space in radiologically normal knees. *Br. J. Rheumatol.* 30:426–428, 1991.
13. Ebrahimi, M., S. Ojanen, A. Mohammadi, M. A. Finnilä, A. Joukainen, H. Kröger, S. Saarakkala, R. K. Korhonen, and P. Tanska. Elastic, viscoelastic and fibril-reinforced poroelastic material properties of healthy and osteoarthritic human tibial cartilage. *Ann. Biomed. Eng.* 47:953–966, 2019.
14. Ebrahimi, M., M. J. Turunen, M. A. Finnilä, A. Joukainen, H. Kröger, S. Saarakkala, R. K. Korhonen, and P. Tanska. Structure-function relationships of healthy and osteoarthritic human tibial cartilage: experimental and numerical investigation. *Ann. Biomed. Eng.* 48:2887–2900, 2020.
15. Favre, J., J. C. Erhart-Hledik, K. Blazek, B. Fasel, G. E. Gold, and T. P. Andriacchi. Anatomically standardized maps reveal distinct patterns of cartilage thickness with increasing severity of medial compartment knee osteoarthritis. *J. Orthop. Res.* 35:2442–2451, 2017.
16. Franz, T., E. M. Hasler, R. Hagg, C. Weiler, R. P. Jakob, and P. Mainil-Varlet. In situ compressive stiffness, biochemical composition, and structural integrity of articular cartilage of the human knee joint. *Osteoarthr. Cartil.* 9:582–592, 2001.
17. Gelse, K., A. Olk, S. Eichhorn, B. Swoboda, M. Schoene, and K. Raum. Quantitative ultrasound biomicroscopy for the analysis of healthy and repair cartilage tissue. *Eur. Cell Mater.* 19:58–71, 2010.
18. Hadjab, I., S. Sim, S. S. Karhula, S. Kauppinen, M. Garon, E. Quenneville, P. Lavigne, P. P. Lehenkari, S. Saarakkala, and M. D. Buschmann. Electromechanical properties of human osteoarthritic and asymptomatic articular cartilage are sensitive and early detectors of degeneration. *Osteoarthr. Cartil.* 26:405–413, 2018.
19. Hui Mingalone, C. K., Z. Liu, J. M. Hollander, K. D. Garvey, A. L. Gibson, R. E. Banks, M. Zhang, T. E. McAlindon, H. C. Nielsen, I. Georgakoudi, and L. Zeng. Bioluminescence and second harmonic generation imaging reveal dynamic changes in the inflammatory and collagen landscape in early osteoarthritis. *Lab. Invest.* 98:656–669, 2018.
20. Huynh, R. N., G. Nehmetallah, and C. B. Raub. Noninvasive assessment of articular cartilage surface damage using reflected polarized light microscopy. *J. Biomed. Opt.* 22:65001, 2017.
21. Huynh, R. N., G. Nehmetallah, and C. B. Raub. Mueller matrix polarimetry and polar decomposition of articular cartilage imaged in reflectance. *Biomed. Opt. Express*. 12:5160–5178, 2021.
22. Huynh, R. N., B. Pesante, G. Nehmetallah, and C. B. Raub. Polarized reflectance from articular cartilage depends upon superficial zone collagen network microstructure. *Biomed. Opt. Express*. 10:5518–5534, 2019.
23. Ishihara, M., M. Sato, N. Kaneshiro, G. Mitani, S. Sato, J. Mochida, and M. Kikuchi. Development of a diagnostic system for osteoarthritis using a photoacoustic measurement method. *Lasers Surg. Med.* 38:249–255, 2006.
24. Johansson, A., T. Sundqvist, J.-H. Kuiper, and P. Å. Öberg. A spectroscopic approach to imaging and quantification of cartilage lesions in human knee joints. *Phys. Med. Biol.* 56:1865, 2011.
25. Jurvelin, J. S., T. Räsänen, P. Kolmonen, and T. Lyyra. Comparison of optical, needle probe and ultrasonic techniques for the measurement of articular cartilage thickness. *J. Biomech.* 28:231–235, 1995.
26. Karjalainen, K., P. Tanska, S. C. Sibole, S. Mikkonen, W. Herzog, R. Korhonen, and E. K. Moo. Effect of cells on spatial quantification of proteoglycans in articular cartilage of small animals. *Connect Tissue Res.* 63:603–614, 2022.
27. Kashimura, Y., R. Matsuda, N. Yamato, and M. Hashimoto. Second-harmonic generation arthroscope with integrated femtosecond Yb fiber laser. , 2022.at <https://opg.optica.org/abstract.cfm?uri=CLEOPR-2022-P_CM15_07>
28. Kiyomatsu, H., Y. Oshima, T. Saitou, T. Miyazaki, A. Hikita, H. Miura, T. Iimura, and T. Imamura. Quantitative SHG imaging in osteoarthritis model mice, implying a diagnostic application. *Biomed. Opt. Express*. 6:405–420, 2015.
29. Kleemann, R. U., D. Krocker, A. Cedraro, J. Tuischer, and G. N. Duda. Altered cartilage mechanics and histology in knee osteoarthritis: relation to clinical assessment (ICRS Grade). *Osteoarthr. Cartil.* 13:958–963, 2005.
30. Kumar, R., K. M. Grønhaug, C. L. Davies, J. O. Drogset, and M. B. Lilledahl. Nonlinear optical microscopy of early stage (ICRS Grade-I) osteoarthritic human cartilage. *Biomed. Opt. Express*. 6:1895–1903, 2015.
31. Laasanen, M. S., J. Töyräs, J. Hirvonen, S. Saarakkala, R. K. Korhonen, M. T. Nieminen, I. Kiviranta, and J. S. Jurvelin. Novel

mechano-acoustic technique and instrument for diagnosis of cartilage degeneration. *Physiol. Meas.* 23:491–503, 2002.
32. Lyyra, T., I. Kiviranta, U. Väätäinen, H. J. Helminen, and J. S. Jurvelin. In vivo characterization of indentation stiffness of articular cartilage in the normal human knee. *J. Biomed. Mater. Res.* 48:482–487, 1999.
33. Mäkelä, J. T. A., Z. S. Rezaeian, S. Mikkonen, R. Madden, S.-K. Han, J. S. Jurvelin, W. Herzog, and R. K. Korhonen. Site-dependent changes in structure and function of lapine articular cartilage 4 weeks after anterior cruciate ligament transection. *Osteoarthr. Cartil.* 22:869–878, 2014.
34. Mansfield, J. C., V. Mandalia, A. Toms, C. P. Winlove, and S. Brasselet. Collagen reorganization in cartilage under strain probed by polarization sensitive second harmonic generation microscopy. *J. R. Soc. Interface*. 16:20180611, 2019.
35. Moo, E. K., Z. Abusara, N. A. Abu Osman, B. Pingguan-Murphy, and W. Herzog. Dual photon excitation microscopy and image threshold segmentation in live cell imaging during compression testing. *J. Biomech.* 46:2024–2031, 2013.
36. Moo, E. K., Y. Al-Saffar, T. Le, R. A. Seerattan, B. Pingguan-Murphy, R. K. Korhonen, and W. Herzog. Deformation behaviors and mechanical impairments of tissue cracks in immature and mature cartilages. *J. Orthop. Res.* 40(9):2103–12, 2021.
37. Moo, E. K., M. Amrein, M. Epstein, M. Duvall, N. A. Abu Osman, B. Pingguan-Murphy, and W. Herzog. The properties of chondrocyte membrane reservoirs and their role in impact-induced cell death. *Biophys. J.* 105:1590–1600, 2013.
38. Moo, E. K., M. Ebrahimi, S. C. Sibole, P. Tanska, and R. K. Korhonen. The intrinsic quality of proteoglycans, but not collagen fibres, degrades in osteoarthritic cartilage. *Acta Biomater.* 153:178–189, 2022.
39. Moo, E. K., S. K. Han, S. Federico, S. C. Sibole, A. Jinha, N. A. Abu Osman, B. Pingguan-Murphy, and W. Herzog. Extracellular matrix integrity affects the mechanical behaviour of in-situ chondrocytes under compression. *J. Biomech.* 47:1004–1013, 2014.
40. Moo, E. K., and W. Herzog. Unfolding of membrane ruffles of in situ chondrocytes under compressive loads. *J. Orthop. Res.* 35:304–310, 2017.
41. Moo, E. K., S. C. Sibole, S. Federico, R. K. Korhonen, and W. Herzog. Microscale investigation of the anisotropic swelling of cartilage tissue and cells in response to hypo-osmotic challenges. *J. Orthop. Res.* 2023. https://doi.org/10.1002/jor.25657.
42. Moo, E. K., S. C. Sibole, S. K. Han, and W. Herzog. Three-dimensional micro-scale strain mapping in living biological soft tissues. *Acta Biomater.* 70:260–269, 2018.
43. Moo, E. K., P. Tanska, S. Federico, Y. Al-Saffar, W. Herzog, and R. K. Korhonen. Collagen fibres determine the crack morphology in articular cartilage. *Acta Biomater.* 2021. https://doi.org/10.1016/j.actbio.2021.03.031.
44. Niederauer, G. G., G. M. Niederauer, L. C. Cullen, K. A. Athanasiou, J. B. Thomas, and M. Q. Niederauer. Correlation of cartilage stiffness to thickness and level of degeneration using a handheld indentation probe. *Ann. Biomed. Eng.* 32:352–359, 2004.
45. Novakofski, K. D., S. L. Pownder, M. F. Koff, R. M. Williams, H. G. Potter, and L. A. Fortier. High-resolution methods for diagnosing cartilage damage in vivo. *Cartilage*. 7:39–51, 2016.
46. Novakofski, K. D., R. M. Williams, L. A. Fortier, H. O. Mohammed, W. R. Zipfel, and L. J. Bonassar. Identification of cartilage injury using quantitative multiphoton microscopy. *Osteoarthr. Cartil.* 22:355–362, 2014.
47. Park, S. H., J. M. Goo, and C.-H. Jo. Receiver operating characteristic (ROC) curve: practical review for radiologists. *Korean J. Radiol.* 5:11–18, 2004.
48. Pedregosa, F., G. Varoquaux, A. Gramfort, V. Michel, B. Thirion, O. Grisel, M. Blondel, P. Prettenhofer, R. Weiss, V. Dubourg, J. Vanderplas, A. Passos, D. Cournapeau, M. Brucher, M. Perrot, and É. Duchesnay. Scikit-learn: machine learning in Python. *J. Mach. Learn. Res.* 12:2825–2830, 2011.
49. Plotnikov, S. V., A. M. Kenny, S. J. Walsh, B. Zubrowski, C. Joseph, V. L. Scranton, G. A. Kuchel, D. Dauser, M. Xu, C. C. Pilbeam, D. J. Adams, R. P. Dougherty, P. J. Campagnola, and W. A. Mohler. Measurement of muscle disease by quantitative second-harmonic generation imaging. *J. Biomed. Opt* 13:044018-044018–11, 2008.
50. Saarakkala, S., P. Julkunen, P. Kiviranta, J. Mäkitalo, J. S. Jurvelin, and R. K. Korhonen. Depth-wise progression of osteoarthritis in human articular cartilage: investigation of composition, structure and biomechanics. *Osteoarthr. Cartil.* 18:73–81, 2010.
51. Saarakkala, S., M. S. Laasanen, J. S. Jurvelin, and J. Töyräs. Quantitative ultrasound imaging detects degenerative changes in articular cartilage surface and subchondral bone. *Phys. Med. Biol.* 51:5333, 2006.
52. Schenke-Layland, K., N. Madershahian, I. Riemann, B. Starcher, K.-J. Halbhuber, K. König, and U. A. Stock. Impact of cryopreservation on extracellular matrix structures of heart valve leaflets. *Ann. Thorac. Surg.* 81:918–926, 2006.
53. Sherlock, B. E., J. Chen, J. C. Mansfield, E. Green, and C. P. Winlove. Biophotonic tools for probing extracellular matrix mechanics. *Matrix Biol. Plus*. 2021. https://doi.org/10.1016/j.mbplus.2021.100093.
54. Sibole, S. C., E. K. Moo, S. Federico, and W. Herzog. The protective function of directed asymmetry in the pericellular matrix enveloping chondrocytes. *Ann. Biomed. Eng.* 50:39–55, 2022.
55. Sim, S., A. Chevrier, M. Garon, E. Quenneville, P. Lavigne, A. Yaroshinsky, C. D. Hoemann, and M. D. Buschmann. Electromechanical probe and automated indentation maps are sensitive techniques in assessing early degenerated human articular cartilage. *J. Orthopaedic Res.* 35:858–867, 2017.
56. Sim, S., A. Chevrier, M. Garon, E. Quenneville, A. Yaroshinsky, C. D. Hoemann, and M. D. Buschmann. Non-destructive electromechanical assessment (Arthro-BST) of human articular cartilage correlates with histological scores and biomechanical properties. *Osteoarthr. Cartil.* 22:1926–1935, 2014.
57. Sim, S., I. Hadjab, M. Garon, E. Quenneville, P. Lavigne, and M. D. Buschmann. Development of an electromechanical grade to assess human knee articular cartilage quality. *Ann. Biomed. Eng.* 45:2410–2421, 2017.
58. Spahn, G., H. M. Klinger, M. Baums, U. Pinkepank, and G. O. Hofmann. Reliability in arthroscopic grading of cartilage lesions: results of a prospective blinded study for evaluation of inter-observer reliability. *Arch. Orthop. Trauma Surg.* 131:377–381, 2011.
59. Stoller, P. C., P. M. Celliers, K. M. Reiser, and A. M. Rubenchik. Imaging collagen orientation using polarization-modulated second harmonic generation. , 2002.
60. Wieland, H. A., M. Michaelis, B. J. Kirschbaum, and K. A. Rudolphi. Osteoarthritis—an untreatable disease? *Nat. Rev. Drug Discov.* 4:331–344, 2005.